

# Boron-Free Fibers for Prevention of Acid Induced Brittle Fracture of Composite Insulator GRP Rods

Daniel L. Armentrout, Maciej Kumosa, and Terry S. McQuarrie

**Abstract**—An investigation was performed to determine whether corrosion resistant boron-free E-glass fibers could adequately prevent acid induced brittle fracture failures of high voltage composite insulator rods. Nine different rod compositions were tested at 45% of mechanical failure load in contact with 1 N nitric acid. Rods made out of commonly used E-glass fibers failed mechanically in less than 2 h whereas the rods based on the corrosion resistant boron-free fibers from two different suppliers survived four days of testing with no visible damage to the rods. Differences in resin types had little effect on the times to failure of the rods. Acoustic emission location analysis was also used to determine the location of fiber fractures along the rods. The location analysis revealed significant differences between the rods with the two different types of corrosion resistant fibers. Boron-free fibers with a lower seed (void) concentration exhibited noticeably fewer fiber fractures as measured by acoustic emission in comparison with the high seed boron-free fibers.

**Index Terms**—Brittle fracture, composite (nonceramic) insulators, glass reinforced polymer (GRP) rods, stress corrosion cracking.

## I. INTRODUCTION

COMPOSITE suspension insulators are used in overhead high voltage transmission lines. A composite insulator shown in Fig. 1 relies on a glass fiber reinforced polymer (GRP) composite rod as the principal load bearing component. The GRP rods are manufactured by pultrusion and unidirectional glass fibers are aligned axially and constitute 55 to 60% of the rod by volume. The remainder of the rod is a polymer resin that binds the fibers together. In order to prevent electrical degradation of the GRP rods and provide the required leakage distance, a rubber housing with multiple weathersheds protects the entire surface of the rod. Two metal end-fittings are attached to the ends of the GRP rod, where the energized or hot end is attached to a high voltage line and the cold end is attached to the tower at ground potential. The two main types of suspension insulators are made out of either composites or porcelain. Composite insulators have advantages over porcelain insulators of a high mechanical strength-to-weight ratio, higher damage tolerance, flexibility, impact resistance, and easier installation. However, composite suspension insulators have been susceptible to in-service failures caused by brittle fracture due to stress corro-

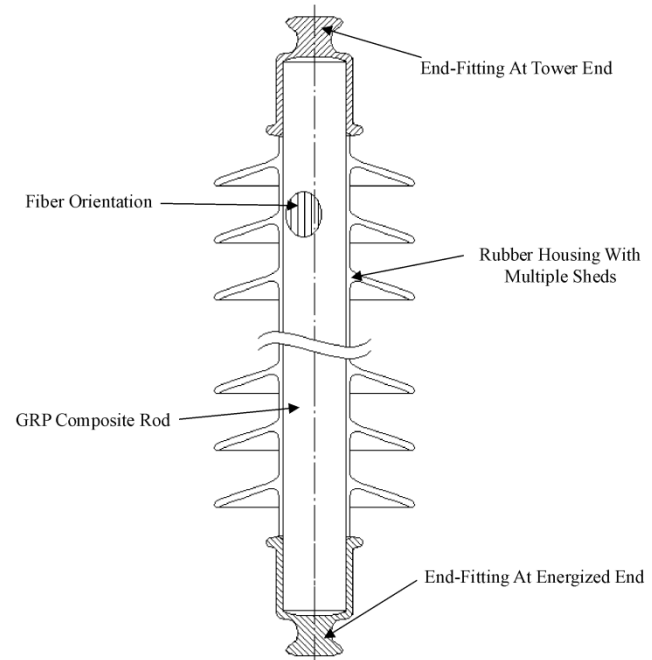


Fig. 1. Schematic of a typical composite insulator.

sion cracking (SCC) of the GRP rods [1]–[20]. SCC failures can occur when composite suspension insulators are mechanically stressed in the presence of a corrosive environment [21]–[30].

Chughtai *et al.* [12] examined actual in-service failed suspension insulators and found nitrates on their fracture surfaces using Fourier transform infrared spectroscopy (FTIR), consistent with presence of  $\text{HNO}_3$ . Kuhl [18] showed that an alternating electrical field at a power delivery voltage could generate nitric acid. Others have postulated that acids can be formed from the chemical components of the epoxy resin [19]. A number of other acids have been postulated as causing SCC [21]–[30]. Different acids have differing rates of SCC in GRP rod materials, but stronger acids of the same type accelerate the SCC process [8]. An acid concentration stronger than  $3.2 \cdot 10^{-4}$  N (3.5 pH) of  $\text{HNO}_3$  seems necessary before SCC can occur [8] in a unidirectional E-glass/polymer composite. The critical acid concentration depends, however, on the type of polymer used.

There are a number of different factors that can affect the failure rates of the insulators. These factors can often be confused by a large variation in failure rates resulting from specimen variations. The crack initiation process was found to be highly dependent on the resin material [29], where vinyl ester, performed better than epoxy, which performed better than polyester. Cyclic loads seem to have a negligible effect on

Manuscript received October 30, 2001. This work was supported by Electric Power Research Institute (EPRI) under Contract EP-P2971/C1399 and in part by Glasforms, Inc.

D. L. Armentrout and M. Kumosa are with the Center for Advanced Materials and Structures, Department of Engineering, University of Denver, Denver, CO 80208 USA (e-mail: darmentr@du.edu; mkumosa@du.edu).

T. S. McQuarrie is with Glasforms, Inc., San Jose, CA 95125 USA (e-mail: terry@glasforms.com).

Digital Object Identifier 10.1109/TPWRD.2003.813599

time to failure of E-glass/polyester rods. A precrack or surface damage of a rod is not necessary to initiate crack propagation since acids can permeate the resins and the pultrusion process leaves exposed fibers on the surface [30].

Alternately, boron-free corrosion resistant fibers named ECRGLAS have been available. ECRGLAS is a registered trademark of Owens-Corning Fiberglas Corporation. Other manufactures also have boron-free corrosion resistant fibers. Boron-free fibers in  $K_1$  experiments have greatly slowed down or even stopped the SCC process [13]. Often though boron-free fibers have not been used as insulators because of their inferior electrical properties. Electric tests performed by McQuarrie [20] have shown that corrosion resistant fibers can have very different electrical properties as measured by a water diffusion electrical test (ANSI 29.11 section 7.4.2). Some corrosion resistant fibers can have as good water diffusion electrical properties as the fibers with boron. The proposed difference in the fibers for the varying electrical properties is a higher concentration of voids within the fibers known as seeds [20]. Seeds are defined as gaseous inclusions within glass in either the molten or solid state.

Acoustic emission (AE) has often been used to monitor core insulator failures because of its high sensitivity to measuring individual fiber fractures [16], [26], and [27]. Signals preferentially propagate along the direction of the glass fibers rather than in other directions [13]. By placing AE sensors at the ends of a GRP rod, location information can be obtained from the time difference of the signals. Undesirable signals from the end fitting, grips, and external sources can be more easily discriminated from fiber fracture signals using two sensors on either end of the specimen.

Location measurements of waves generated in a rod are complicated by the fact that waves of different frequency have different propagation velocities. Waves of different types (longitudinal, flexure, and torsional wave) also have different dependence of velocity with frequency. Wave velocities that vary with frequency have the effect of spreading the wave as it propagates through the rods. For fiber fractures in rods, the longitudinal component is the primary wave generated with a small amount of flexural wave. For higher frequencies, the velocities of the longitudinal and flexural waves are approximately the same. The spreading of a wave as it propagates greater distances through the rod complicates accurately determining the start of the wave. This introduces error in the location measurement of the source of the wave.

## II. EXPERIMENTAL PROCEDURE

### A. Materials Tested

A total of 27 GRP rods of nine different types, 16 mm in diameter were obtained from Glasforms, Inc. The rods were based on three different glass fibers (E-glass with boron, boron-free glass from supplier 1 and boron-free glass from supplier 2) with three different resins. The chemical composition of the fibers tested [20] and the E-glass chemical composition established by ASTM D578-98 standard is given in Table I. All rods passed a dye penetration test (ANSI 29.11 section 7.4.1) [20]. The resins were a modified polyester, epoxy/anhydride, and Bis A vinyl

TABLE I  
GLASS FIBER CHEMICAL COMPOSITION PERCENT BY WEIGHT

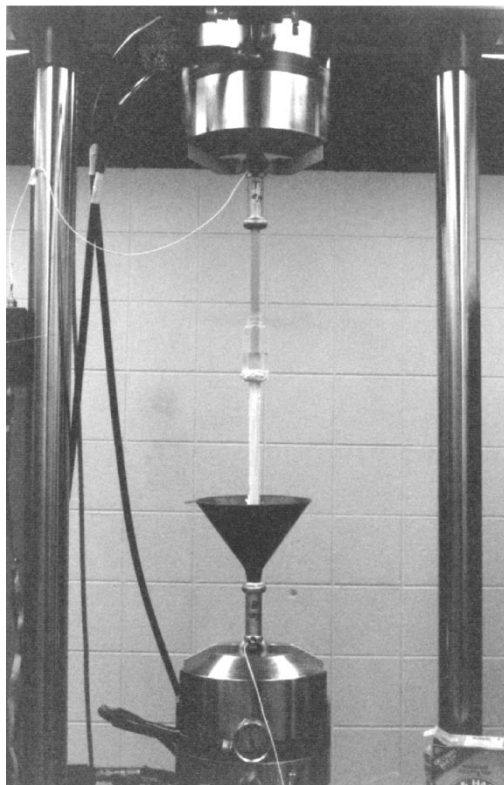
Chemical	ASTM Standard (E-glass)	E-Glass Fibers with Boron	Boron-Free Fibers #1	Boron-Free Fibers #2
SiO <sub>2</sub>	52 to 62	54.5	59.7	59.0
CaO	16 to 25	23.0	21.9	22.6
Al <sub>2</sub> O <sub>3</sub>	12 to 16	14.5	13.6	12.1
B <sub>2</sub> O <sub>3</sub>	0 to 10	6.0	0	0
MgO	0 to 5	0.5	3.3	3.4
Na <sub>2</sub> O and K <sub>2</sub> O	0 to 2	1.0	0.8	0.9
TiO <sub>2</sub>	0 to 1.5	0.5	0.5	1.5
Fluoride	0 to 1.0	0.5	0	0

ester. An insulator manufacturer attached the end fittings to the rods before testing. Prior to the attachment of the end fittings, all specimens were sandblasted and in addition the epoxy/anhydride rods were post-cured for 17 h at 140 °C in order to duplicate the manufacturer's actual processing of the rods. Sandblasting of the GRP rods is usually applied to enhance chemical bonding between the surface of the GRP rod and a housing rubber alloy.

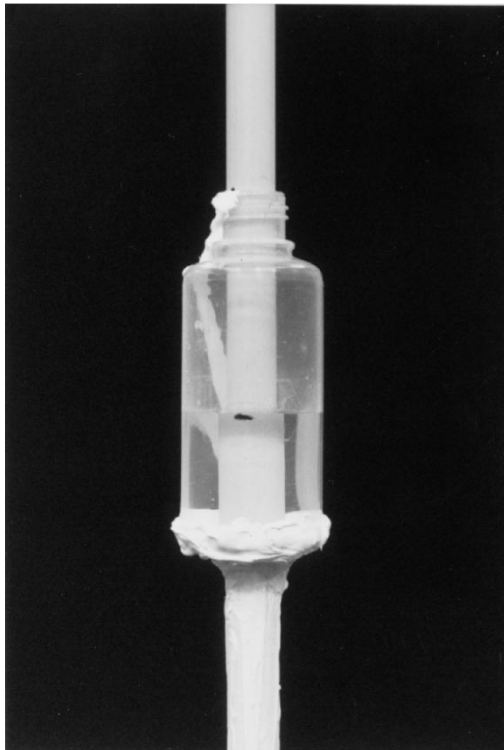
### B. Stress Corrosion Experiments on GRP Rods

Before testing each specimen, a portion of the metal end fitting was machined away to expose the ends of the GRP rods for attaching two AE transducers. Wide band B1025 sensors (Digital Wave Corp.) were used and coupled to the rod ends with vacuum grease. A plastic funnel was attached around the base of the rod to collect any acid that leaked during specimen failure. The funnel was also filled with sodium bicarbonate to neutralize any acid that collected in the funnel. A hole was put in the bottom of a 125-ml bottle and one side of the bottle was cut so the bottle could be placed around a GRP rod. The base of the bottle was sealed to the rod at a location of 0.34 m from the top of 0.78 m long GRP rods. Sealant was applied around the funnel and on the rod between the funnel and bottle to localized the acid attack and prevent acid attack of the end fitting, transducer, and specimen grip. A GRP rod prepared for testing is shown in Fig. 2(a) and a close-up of the acid bottle is shown in Fig. 2(b). In addition, a diagram of the experimental arrangement used in the stress corrosion tests is shown in Fig. 3.

The GRP rods were tested under extremely harsh stress corrosion conditions. The mechanical tensile stress in the rods was 45% of the average tensile strength of the GRP rods. One N HNO<sub>3</sub> acid was used in the tests. Compared with other stress corrosion tests performed by Kumosa *et al.* (stress at 18% of the average tensile strength and  $6.3 \cdot 10^{-2}$  N HNO<sub>3</sub>) [14], [15], [17], the tests conducted in this project were highly accelerated. After the sealant cured, each GRP rod was rapidly, but smoothly loaded in a MTS 880 load frame to 66.47 kN. Immediately after mechanical loading of the specimen, nitric acid was added to the bottle and the test timer started. The level of acid was approximately 40 mm above the bottom of the bottle. The load applied to each rod was maintained until failure or for 96 h, whichever occurred first. The wide band sensors with a frequency range of 20–1500 kHz are able to distinguish between signals from many different AE sources. The frequency range of a fiber fracture can extend up to over 1 MHz although the majority of the signal



(a)



(b)

Fig. 2. GRP rod subjected to the stress corrosion test, (a) GRP rod under tension in the test frame in the process of testing and (b) a close-up of the acid container.

energy is in the range of 50–500 kHz. To minimize pickup of nonfiber break signals, the trigger band pass was set to 50–500 kHz. A separate band pass of 20–4000 kHz was used to record

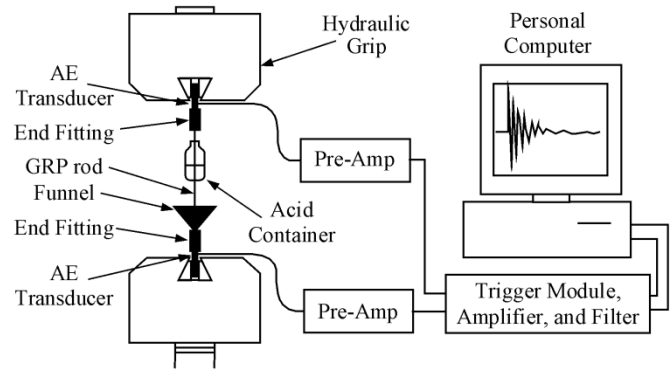


Fig. 3. Test setup diagram used in the stress corrosion experiments on the GRP rods.

signals so that the recorded signal was as close as possible to the signal measured by the transducer. The total gain for the two transducers was 61 dB for the trigger and 55 dB for the recorded signal giving an effective threshold level  $89 \mu\text{V}$  referenced to the transducer.

The signals were measured at 5 MHz per point for 2048 points with 256 points recorded before the trigger. The maximum voltage level was  $\pm 1.0 \text{ V}$  or  $1.78 \text{ mV}$  referenced to the transducer. At a 5-MHz digitization rate, a signal with a high enough frequency ( $>2.5 \text{ MHz}$ ) would be aliased to other frequencies. Since the transducer frequency response rapidly drops off above 1.5 MHz, this adequately reduces frequency aliasing that would occur for frequencies above 2.5 MHz.

The longitudinal wave velocity was measured using pencil lead breaks as an AE source on one end of an E-glass/epoxy rod and was found to be approximately 4700 m/s. This value was assumed for all nine different composite rod materials. The digitization rate and wave velocity gave an ultimate location resolution of about 0.5 mm.

A JEOL 5800 LV scanning electron microscope (SEM) was used for examining the morphology of the GRP rods after the stress corrosion tests. SEM images were obtained in low vacuum mode, which allow for examination of uncoated rods. A backscatter electron detector was used for all SEM images.

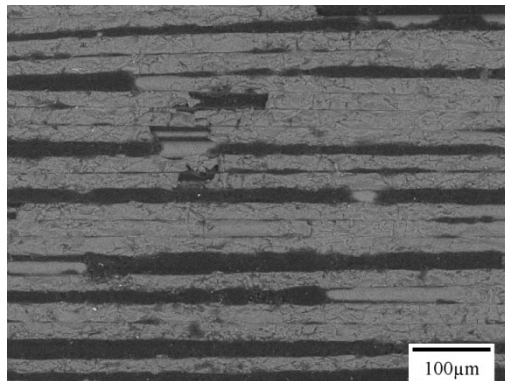
### III. RESULTS AND DISCUSSION

#### A. Failure Times

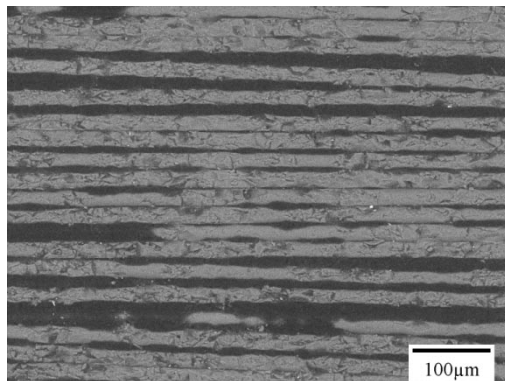
Test failure times for the 27 specimens with nine different materials are shown in Table II. The GRP rods with the widely used E-glass fibers (with boron) all experienced failures in under two hours while the other composite systems with the two boron-free fibers (from suppliers 1 and 2) lasted until the test was stopped after 96 h with no apparent visible damage to the rods. The difference between failure times of the E-glass fibers with boron for the different resins was slight with the polyester based rods performing best for this fiber type. This advantage has some overlap with two vinyl ester tests having longer failure times than the worst polyester. The minor time differences between the resins, however, are insignificant when compared to the data for the corrosion resistant boron-free fibers.

TABLE II  
FAILURE TIMES FROM THE STRESS CORROSION TESTS IN MINUTES

Composite System	Spec. #1	Spec. #2	Spec. #3	Average
1. E-Glass Fibers with Boron/Polyester	101.1	114.4	95.7	103.7
2. E-Glass Fibers with Boron/Epoxy	85.3	94.9	95.0	91.8
3. E-Glass Fibers with Boron/Vinyl Ester	99.7	87.1	97.6	94.8
4. Boron-Free Fiber #1/Polyester	>5760	>5760	>5760	>5760
5. Boron-Free Fiber #1/Epoxy	>5760	>5760	>5760	>5760
6. Boron-Free Fiber #1/Vinyl Ester	>5760	>5760	>5760	>5760
7. Boron-Free Fiber #2/Polyester	>5760	>5760	>5760	>5760
8. Boron-Free Fiber #2/Epoxy	>5760	>5760	>5760	>5760
9. Boron-Free Fiber #2/Vinyl Ester	>5760	>5760	>5760	>5760



(a)

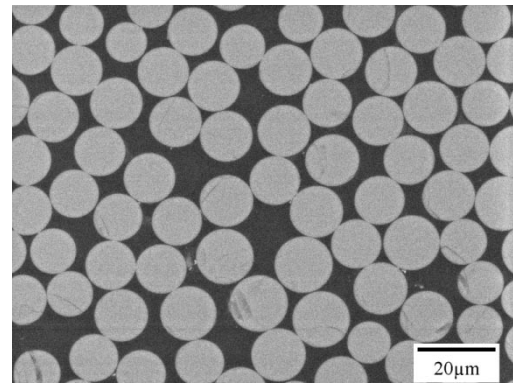


(b)

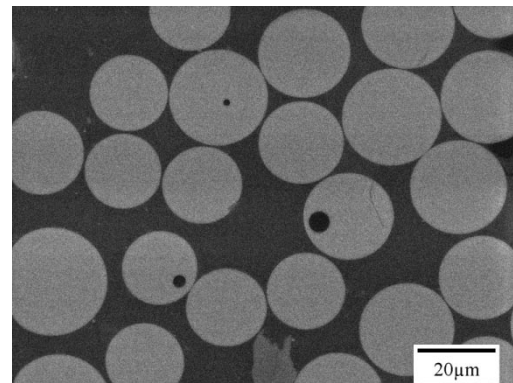
Fig. 4. SEM images of the surface of a GRP rod based on boron-free fibers #1 with modified polyester. (a) Without acid exposure. (b) After acid exposure.

**B. SEM Analysis**

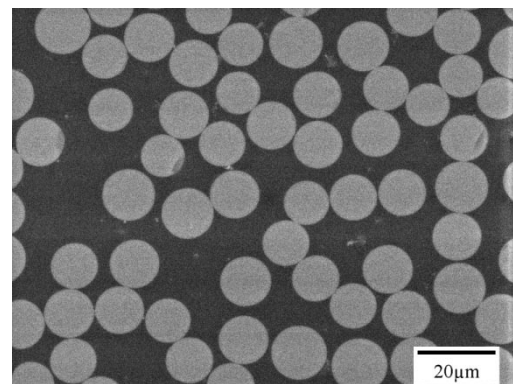
After testing, the surfaces of the GRP rods with the boron-free glass fibers were examined using SEM. The surface morphologies of the rods in the acid exposed and unexposed areas were compared and are shown in Fig. 4(a) and (b) for boron-free fibers #1/polyester GRP rod as an example. Due to the surface damage caused by sandblasting, no differences were observed between the acid exposed and unexposed regions. A



(a)



(b)



(c)

Fig. 5. SEM images of polished cross sections of three GRP rods based on polyester with, (a) E-glass fibers with boron. (b) Boron-free fibers #1. (c) Boron-free fibers #2.

small number of acid induced fiber fractures could have easily occurred in the fibers on the surface and not be distinguished from the significant damage caused by sandblasting.

Polished rod cross sections of the three different types of the fibers are shown in Fig. 5(a)–(c). Since all of these images were taken at the same magnification, an obvious difference between the fibers is their average diameter. The boron-free fibers #1 are approximately 20 µm in diameter while the boron-free fibers #2 and the fibers with boron have a diameter of about 14 µm. Another major difference between these fibers is the presence of voids in some of the fibers. These voids or seeds were commonly observed in the boron-free fibers #1 while none were observed in the fibers with boron or the boron-free fibers #2.

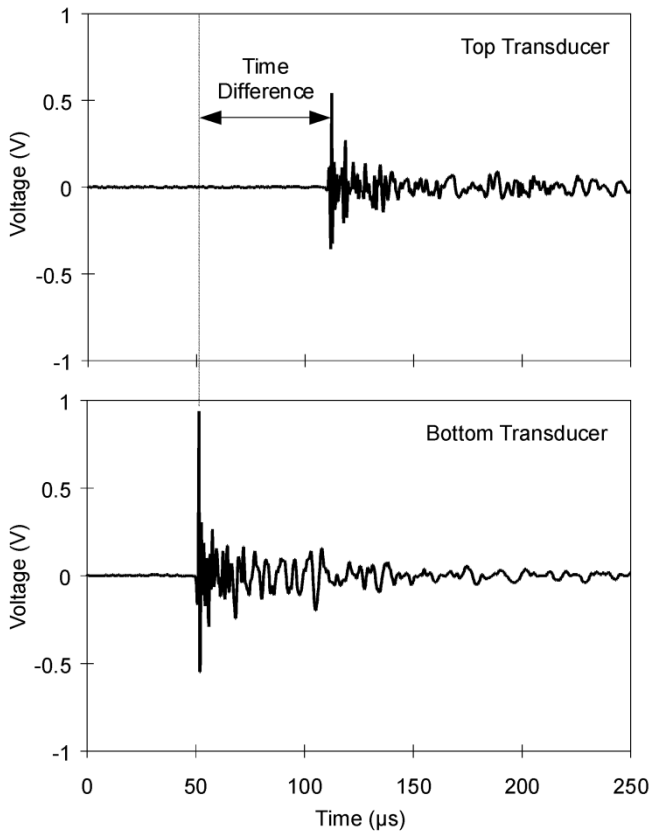


Fig. 6. AE signal generated by a fiber fracture 0.51 m from the top end of a GRP rod.

### C. Verification of the AE Location Measurements

In addition to the stress corrosion tests on the GRP rods with the three different types of glass fibers, verification experiments of the AE location analysis technique were also performed on 16 mm diameter GRP rods made from E-glass fibers with boron in epoxy resin. The rods had a defect (a short transverse precrack) cut into the specimens at 0.41, 0.46, and 0.51 m from the top of 0.72 m long rods. This time, the rods were not sandblasted and had only one main crack initiation site. The rates of SCC were significantly slowed down by testing these specimens under less extreme conditions in comparison with the tests described in Section III-A. This allowed for less saturation of the AE system and less multiple fiber fractures recorded as one digital sample (sample duration of 409.6  $\mu\text{s}$ ). The tests were performed at an applied load of 26.73 kN (18% of failure load) with a more dilute nitric acid of 1.2 pH ( $6.3 \cdot 10^{-2}$  N). These test parameters gave an average failure time for six specimens of approximately 46 h. No tests were performed with crack initiation sites in the middle of the GRP rods, which cause simultaneous arrival times, since most external AE noise sources have simultaneous arrival times, which give a middle of the rod the middle of the GRP rods since most external AE sources cause signals location. Distances were all measured from the top of the specimen.

A wave generated by a fiber break in a rod is shown in Fig. 6 from a defect 0.15 m away from the middle of the rod (0.51 m from the top). This wave has a fairly abrupt step in voltage at

the start of the wave. The dispersion of the signal traveling the extra 0.30-m distance in the rod is also of minor significance in determining the start of the wave. Since the start of the wave can be easily identified using a simple threshold crossing, more elaborate location schemes need not be used.

There were several criteria used to distinguish between fiber fracture signals and other signals. The following types of signals were rejected: 1) any signal that had a location outside the rod length, 2) signals that did not have a threshold crossing on both channels, 3) signals with an early initial threshold crossing, 4) signals characteristic of electromagnetic interference. Signals rejected by criteria #3 were generated either by low frequency mechanical vibrations or multiple signals coming in so close together in time that the start of the signal was missed by the AE system. Signals with a threshold crossing 41.2  $\mu\text{s}$  before the system trigger were rejected. When electrical interference signals were present, fiber fracture signals characterized by the shape of the signal shown in Fig. 6 were separated out manually from the interference signals.

Using the threshold crossing as the method of determining the start of the signal and taking 4700 m/s as the longitudinal wave velocity, the location calculation gave a distribution of fiber fracture signals shown in Fig. 7(a) for the first 10 000 signals from the specimens with precracks at 0.41, 0.46, and 0.51 m from the top of the rods. Fig. 7(b) shows the location distribution for the fracture signals from the entire test.

From the data presented in Fig. 7(a), signals are located near the initial transverse precracks. Examinations of the specimens after failure showed that initially stress corrosion cracks propagated along the precrack. As the test progressed, additional planar cracks were observed developing at other sites and along longitudinal splits on both sides of the initial transverse cracks. Therefore, AE sources should spread out around the initial precrack location as the test progresses. This phenomenon can be clearly seen in Fig. 7(b) for all of the signals measured from the tests for three different precrack locations. The data presented in Fig. 7 clearly demonstrate that the location of fiber fractures can be very accurately determined. In addition, the transition from planar fracture to multiple fractures with axial splits can be easily detected using the location technique. In summary, the AE location analysis can be applied to monitor all stages of the stress corrosion fracture process in the GRP rods.

### D. AE Analysis of SCC in the GRP Rods

The failure time data presented in Table II alone are not enough to determine if the boron-free fibers from both suppliers are entirely immune to SCC. If given enough time, the fibers could still stress corrode under the extreme stress corrosion conditions used in the experiment described in Section III-A. The AE location analysis presented in the section before was used to determine the number and location of fiber fractures that occurred during the stress corrosion tests. The filtered AE signals from the tests performed on the rods were analyzed to obtain the location of the fiber fracture signals. Table III contains a listing of the total number of AE signals from each specimen and the number of signals generated in the region exposed to acid on the rods.

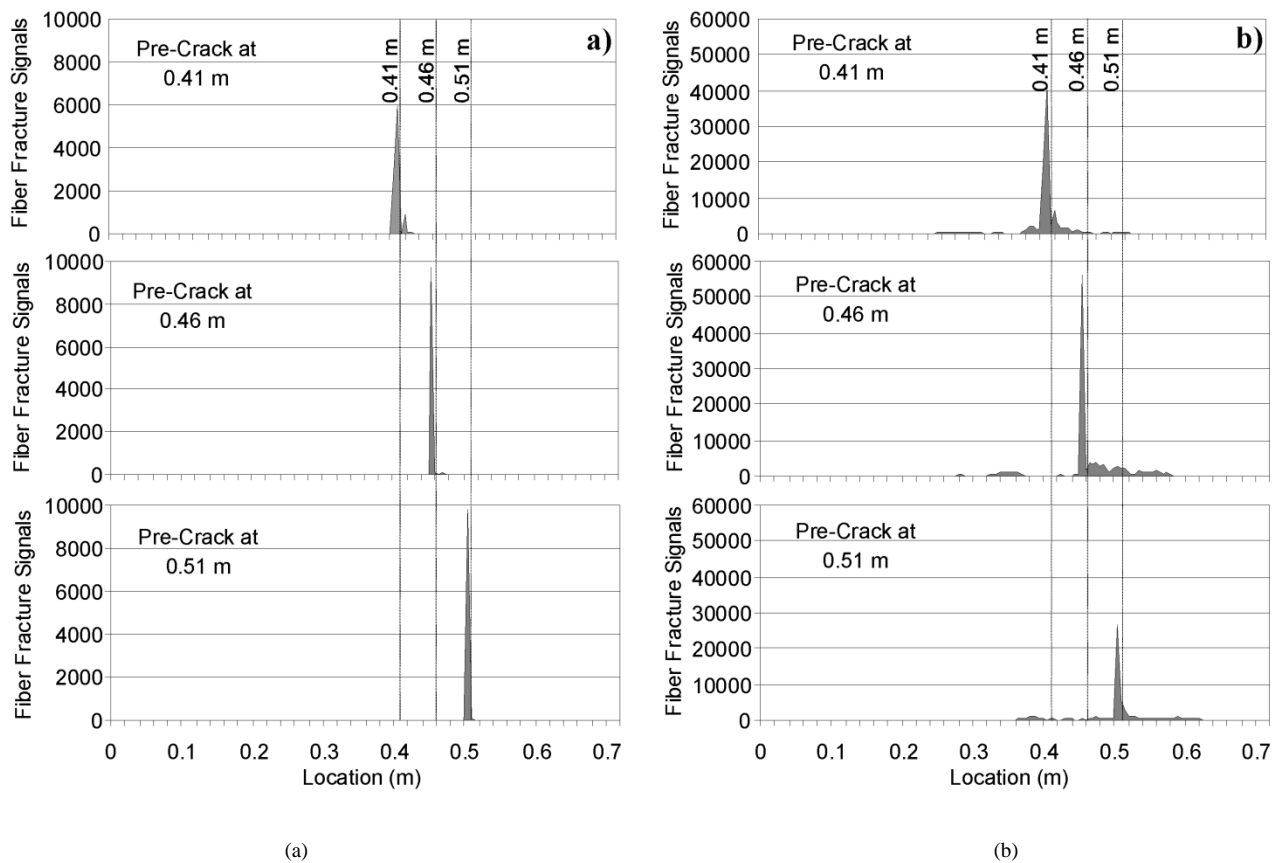


Fig. 7. Location of stress corrosion cracking in E-glass/epoxy rods with short precracks at 0.41, 0.46, and 0.51 m from the top end of the rods (a) initial stages of SCC with fracture perpendicular to the rod axis (first 10 000 signals). (b) Fractures from the entire test that occur along the rods at different locations.

When specimen #1 from the E-glass with boron/polyester rods was tested, the data acquisition rate was too high to be processed by the AE system, causing the system to lock up and the loss of the data. Rather than changing the testing conditions to slow the failure process, an alternative was to reduce the maximum data acquisition rate for the AE system by increasing the amount of graphics being displayed by the AE computer system. With the computer busy displaying graphics it could not record AE data as fast and a representative selection of the total number of signals generated in the specimen was obtained.

The total number of fibers in a GRP rod can be estimated from the average fiber diameter and the volume fraction of fibers. Assuming a 55% fiber volume and knowing that the rod cross section is 201 mm<sup>2</sup>, the approximate number of fibers was estimated to be 352 000 for 20 μm diameter fibers and 718 000 for 14-μm diameter fibers. With slow data acquisition rates, the AE system can capture the majority of the fiber fracture signals [16], [26], [27]. Since determining the location of AE signals was viewed to be more important than capturing every signal, the maximum data acquisition rate of the AE system was reduced by displaying more graphics on the computer screen. Therefore, the numbers for fiber fractures in Table III for the E-glass fibers with boron are lower than they would have been if every signal was captured. For the tests with the two types of boron-free fibers, the fiber fracture rate was low enough that the AE system could capture nearly every signal.

Fig. 8(a) shows a graph of fiber fracture signals versus time for E-glass with boron/polyester specimen #2. A fiber break lo-

TABLE III  
AE FROM FIBER FRACTURES

Composite System	Measured Number of Fiber Fracture Signals			Fiber Fracture Signals within Acid Region		
	Spec. #1	Spec. #2	Spec. #3	Spec. #1	Spec. #2	Spec. #3
1. E-Glass Fibers with Boron/Polyester	*	72686	102265	*	53172	89559
2. E-Glass Fibers with Boron/Epoxy	13525	36858	26726	8844	25038	20158
3. E-Glass Fibers with Boron/Vinyl Ester	7654	39361	39135	4433	32092	24561
4. Boron-Free Fiber #1/Polyester	1187	1742	2099	860	1079	912
5. Boron-Free Fiber #1/Epoxy	124	3	12	100	1	12
6. Boron-Free Fiber #1/Vinyl Ester	48	14	539	38	11	230
7. Boron-Free Fiber #2/Polyester	0	2	0	0	0	0
8. Boron-Free Fiber #2/Epoxy	0	0	0	0	0	0
9. Boron-Free Fiber #2/Vinyl Ester	0	0	0	0	0	0

\*AE data were lost from this test.

cation graph for the first 10 000 signals is shown in Fig. 8(b). Finally, all fiber break location signals from the test are shown in the location graph of Fig. 8(c). For reference, the diagram of the specimen is included at the top of Fig. 8(b) and (c).

Initially, the rate of fiber fractures was slow [see Fig. 8(a)], but once a well-defined crack began to propagate across the spec-

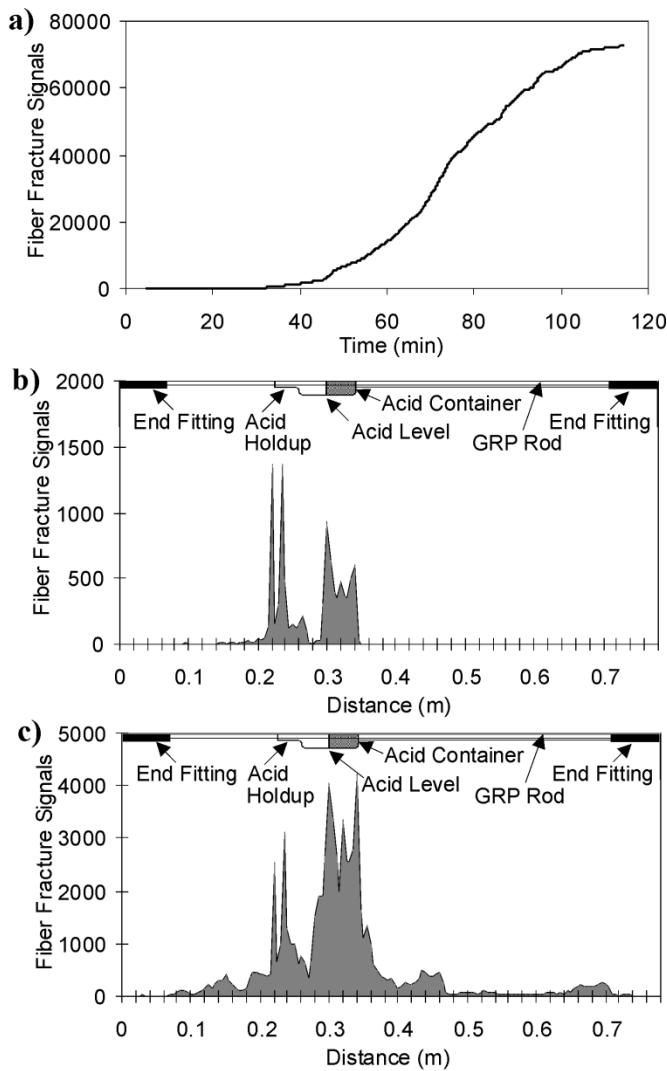


Fig. 8. AE data shown from an E-glass/polyester rod specimen #2, (a) AE fiber fracture signals versus time. (b) Location of the fiber fracture signals along the rod for the first 10 000 signals. (c) Location of the fiber fracture signals for all signals during the test.

imen, the fracture rate increased. Since there were numerous crack initiation sites, many cracks were growing at many locations at the same time. The fracture rate increased to the saturation rate of the AE system. Splitting along the fibers caused a reduction in the fiber fracture rate and reduced the sensitivity of the AE system to fiber fractures. Once a split occurred, the stress concentration at the crack tips reduced, and acid was taken away from the crack tip by either flowing down the rod or wicking up the rod. New crack initiation sites were started as the acid attacks previously unexposed areas and old crack locations stop because of the drop in stress concentration. Near the end of the test, the fracture rate slowed because splits damaged the silicon sealant and acid flows out of the container and because specimen damage reduces sensitivity of the AE system to fiber fractures. Enough acid remained on the rod to continue the process to specimen failure.

Initially, the acid contacted the rods at about 0.22 m from the top (above the acid bottle). The acid flowed down the rod into the container and accumulated at the bottom (0.34 m). Even

though the acid contacted the higher region of the rod for only a short period of time, some acid residue was left behind that concentrated as it dried. The concentrated acid caused a significant number of fiber fractures.

The majority of the signals in Fig. 8(b) occur in the acid region (0.30 to 0.34 m). However, on either side of this region, extending about 0.1 m, a significant number of fiber fractures occurred. Due to the surface roughness, it is likely that some acid residue remained after filling the container and some acid penetrated down into the silicone sealant. The peaks at 0.22 and 0.23 m are near the location of the top of the container. The bottle used to contain the acid around the rod had a top that was just slightly larger in diameter than the rod. During some tests, small drops of acid were held up between the neck of the bottle and the rod. Over time, liquid in the hold up region would evaporate and concentrate the acid. Acid in the hold up region was responsible for fiber fractures measured at 0.22 and 0.23 m. Examination of the failed rod revealed a significant crack at the location of the acid holdup region.

The additional fractures occurring later, as shown in Fig. 8(c), spread out over the entire length of the rod. As the rod gets closer to failure, splitting allowed the acid to penetrate both higher by wicking up the rod and lower along the specimen. Near the end of the test, acid pools up at the bottom of the rod just above the end fitting causing additional fiber fractures in the 0.65 to 0.71 m range. The relative peak heights at 0.22–0.23 m compared to the peaks between 0.30–0.34 m are reduced in Fig. 8(c) compared to Fig. 8(b). Since only small drops of acid were responsible for the peaks at 0.22–0.23 m, the rate of fracture decreased as the test progressed compared to the main volume of acid.

For the rods based on boron-free fibers #1, fiber fracture signals were recorded in every test. More signals were obtained from the fibers in polyester resin than in the other two resins. At this time, no reason is known why the rods based on the polyester resin had more signals than in the other two cases. For most tests with the boron-free fibers #1, the fiber fracture rate decreased with time. A fiber fracture signals versus time plot is shown in Fig. 9(a) with the corresponding location plot in Fig. 9(b) for boron-free fibers #1/polyester specimen #2. The location plot reveals a concentration of signals near the location of the acid. Almost no signals were recorded from the end fitting regions. Other regions outside the acid and away from the end fittings had differing numbers of signals. Some of these signals could have been caused by fiber damage during sandblasting or fiber seed fractures.

Specimen #1 of boron-free fibers #1/polyester had a fiber fracture signal rate curve clearly different from the curve shown in Fig. 9(a). Its fiber fracture signal rate curve is shown in Fig. 10(a). During the first half of this curve, it is very similar to the slowing fiber fracture signal rate shown in Fig. 9(a). After the first half of the test, the fiber fracture signal rate increased. The location plot shown in Fig. 10(b) for the first half of the test is also very similar to the location plot shown in Fig. 9(b). However, during the second half of this test, the location plot [Fig. 10(c)] shows a large number of signals coming from the acid holdup region (0.25 m). After testing, the rod was optically examined near the region of the high AE activity and a slight yellowing of the rod surface was observed.

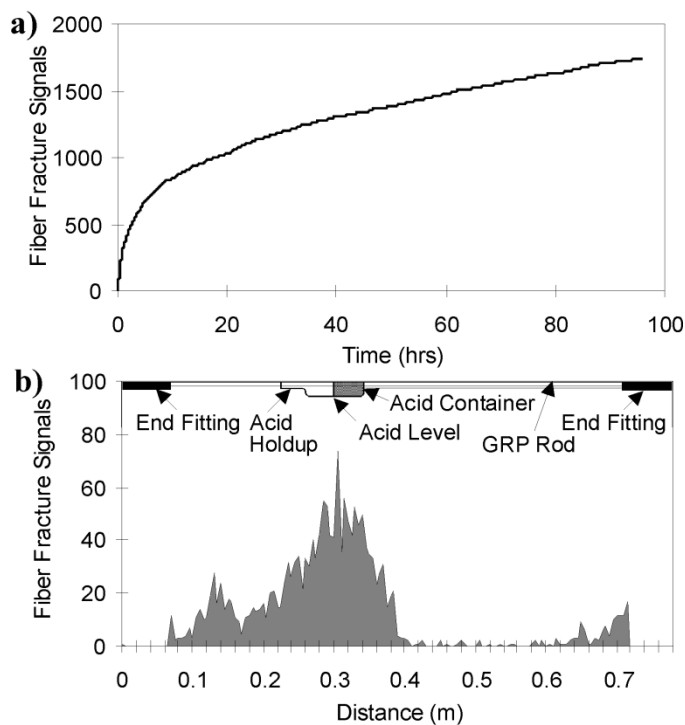


Fig. 9. AE data for a rod with boron-free fibers #1/polyester specimen #2. (a) AE fiber fracture signals versus time. (b) Location of the fiber fracture signals recorded during the test.

Several stress corrosion cracks were found with the SEM in the region of the high AE activity and one is shown in the center of Fig. 11. Other fiber fractures from sandblasting are also shown around the corrosion crack.

The results from the tests on the rods with the boron-free fibers with high seeds (#1) and polyester clearly demonstrate that the stress corrosion cracking in this type of composite is possible especially if highly concentrated acids are involved. The higher concentration of seeds in boron-free fibers #1 added some fracture signals at the sites of seeds.

In the tests performed on the rods with boron-free fibers #2 (low seed), no detectable fiber fractures from the acid region were recorded. Only two fiber fractures were detected in all of the tests combined.

#### IV. CONCLUSIONS

The GRP rods based on boron-free fibers are significantly more resistant to stress corrosion cracking in 1 N nitric acid solutions under high tensile loads (45% of failure) than the rods with the E-glass fibers with boron. While all of the GRP rods that had fibers with boron failed in less than 2 h, the specimens with the two different types of boron-free fibers held load for 96 h with no visible sign of damage. Since the most common glass fibers being used in composite insulators have boron, the boron-free fibers would offer an advantage of being more corrosion resistant.

The SCC in GRP rods can be accurately monitored by AE. Location information can be used to monitor SCC in GRP rods as well as the initiation of stress corrosion damage along the rods.

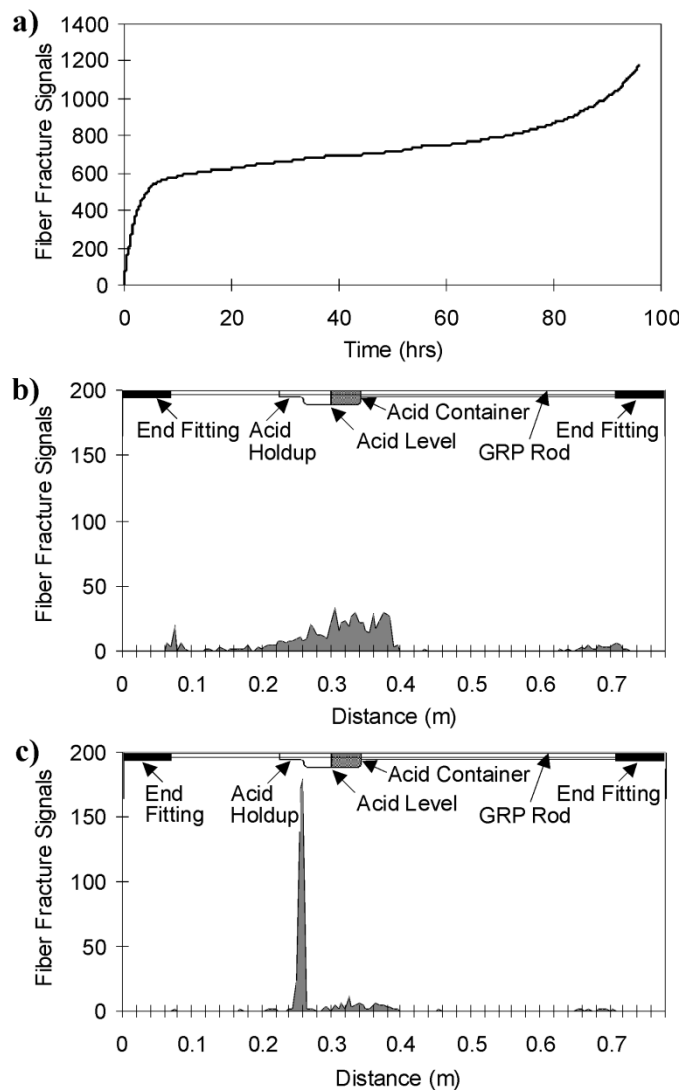


Fig. 10. Plots are shown for a rod with boron free fibers #1/polyester specimen #1 of (a) AE fiber fracture signals versus time. (b) Location of the fiber fracture signals for the first 48 h of the test. (c) Location of the fiber fracture signals for the second 48 h of the test.

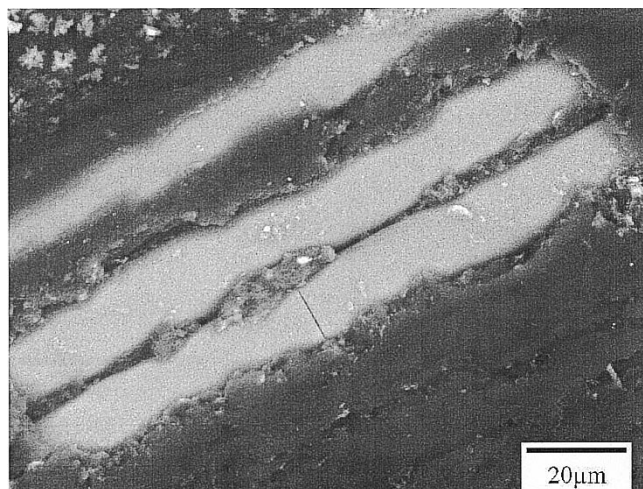


Fig. 11. Stress corrosion cracking is shown in the center of this image of a low seed boron-free (#1)/polyester composite rod.

Under extreme SCC conditions, boron-free fibers with high seed counts can experience SCC. In an area where the 1 N nitric acid could be concentrated, small cracks began to grow as measured by AE activity. This would imply that a threshold level of acid concentration exists for crack growth in the boron-free fibers at a concentration level above 1 N HNO<sub>3</sub>. It is unlikely that in service, the acid concentration could be high enough to initiate corrosion in boron-free fibers.

Not all boron-free fibers have the same resistance to stress corrosion cracking. The GRP rods based on the boron-free fibers with high seed concentration generated significantly more fiber fracture signals than the GRP rods with the low seed boron-free fibers. However, both boron-free fiber types were much more corrosion resistant than the fibers with boron.

#### ACKNOWLEDGMENT

The authors are grateful to Dr. J. Stringer of EPRI for his support of this study and L. Kumosa for his work on this document.

#### REFERENCES

- [1] B. Noble, S. J. Harris, and M. J. Owen, "Stress corrosion cracking of GRP pultruded rods in acid environments," *J. Mater. Sci.*, vol. 18, pp. 1244–1254, 1983.
- [2] S. J. Harris, B. Noble, and M. J. Owen, "Metallographic investigation of the damage caused to GRP by the combined action of electrical, mechanical, and chemical environments," *J. Mater. Sci.*, vol. 19, pp. 1596–1604, 1984.
- [3] A. Akhtar, J. S. Nadeau, J. Y. Wang, D. P. Romily, and C. Taggart, "Brittle fracture of nonceramic insulators," Prepared by the British Columbia Hydro and Power Authority, Report for the Canadian Electrical Association (186 T 350), 1986.
- [4] M. J. Owen, S. J. Harris, and B. Noble, "Failure of high voltage electrical insulators with pultruded glass fiber-reinforced plastic cores," *Composites*, vol. 17, pp. 217–226, 1986.
- [5] A. Akhtar and J. Y. Wong, "Failure analysis of brittle fracture in nonceramic insulators," *J. Comp. Tech. Res.*, vol. 9, pp. 95–100, 1987.
- [6] M. Kumosa *et al.*, "Micro-fracture mechanisms in glass/polymer insulator materials under combined effects of electrical, mechanical and environmental stresses," EPRI and the WAPA, Oregon Grad. Inst. of Sci. and Tech., Final Report to the Bonneville Power Admin., 1994.
- [7] M. Kumosa, Q. Qiu, E. Bennett, C. Ek, T. S. McQuarrie, and J. M. Braun, "Brittle fracture of nonceramic insulators," in *Proc. Fracture Mech. Hydroelectric Power Syst. Symp.*: Canadian Committee for Research on the Strength and Fracture of Materials (CSFM), BC Hydro, 1994, pp. 235–254.
- [8] Q. Qiu, "Brittle fracture mechanisms of glass fiber reinforced polymer insulators," Ph.D. dissertation, Oregon Grad. Inst. of Sci. & Tech., 1995.
- [9] M. Kumosa and Q. Qiu, "Failure analysis of composite insulators (failure investigation of 500 kv nonceramic insulators for pacific gas & electric company)," Final Rep. to the Pacific Gas and Electric Co., Dept. Eng., Univ. Denver, 1996.
- [10] M. Kumosa, H. Shankara Narayan, Q. Qiu, and A. Bansal, "Brittle fracture of nonceramic suspension insulators with epoxy cone end-fittings," *Comp. Sci. Tech.*, vol. 57, pp. 739–751, 1997.
- [11] Interviews with Maciej Kumosa, "Research of brittle fractures in composite insulators," *Insulator News Market Rep.*, pp. 46–51, July/Aug. 1997.
- [12] A. R. Chughtai, D. M. Smith, and M. Kumosa, "Chemical analysis of a field-failed composite suspension insulator," *Comp. Sci. Tech.*, vol. 58, pp. 1641–1647, 1998.
- [13] T. Ely, D. Armentrout, and M. Kumosa, "Evaluation of stress corrosion properties of pultruded glass fiber/polymer composite materials," *J. Comput. Math.*, vol. 35, pp. 751–773, 2001.
- [14] M. Kumosa *et al.*, "Micro-fracture mechanisms in glass/polymer insulator materials under the combined effect of mechanical, electrical and environmental stresses," Final Rep. to BPA, APA, PG&E, WAPA and NRECA, Univ. Denver, Dec. 1998.
- [15] D. Armentrout, T. Ely, S. Carpenter, and M. Kumosa, "An investigation of brittle fracture in composite materials used for high voltage insulators," *J. Acoust. Emission*, vol. 16, pp. S10–S18, 1998.
- [16] T. Ely and M. Kumosa, "The stress corrosion experiments on an e-glass/epoxy unidirectional composite," *J. Comput. Math.*, vol. 34, no. 10, pp. 841–878, 2000.
- [17] S. H. Carpenter and M. Kumosa, "An investigation of brittle fracture of composite insulator rods in an acid environment with either static or cyclic loading," *J. Math. Sci.*, vol. 35, pp. 4465–4476, 2000.
- [18] M. Kuhl, "FRP rods for brittle fracture resistant composite insulators," *IEEE Trans. Dielect. Elect. Insulation*, vol. 8, pp. 182–190, Apr. 2001.
- [19] C. de Tourreil, L. Pargamin, G. Thévenet, and S. Prat, "Brittle fracture of composite insulators: why and how they occur," in *Power Eng. Soc. Summer Meeting*, vol. 4, 2000, pp. 2569–2574.
- [20] T. S. McQuarrie, "Improved dielectric & brittle fracture resistant core rods for nonceramic insulators," in *Proc. World Congr. Insulator Technol. Year 2000 Beyond*, Barcelona, Spain, Nov. 14–17, 1999.
- [21] A. G. Metcalfe and G. K. Schmitz, "Mechanism of stress corrosion in E glass filaments," *Glass Tech.*, vol. 13, p. 5, 1972.
- [22] J. F. Mandell, D. D. Huang, and F. J. McGarry, "Tensile fatigue performance of glass fiber dominated composites," *Comp. Tech. Rev.*, vol. 3, pp. 96–102, 1981.
- [23] D. Hull, M. Kumosa, and J. N. Price, "Stress corrosion of aligned glass fiber-polyester composite material," *Materials Science and Technology*, vol. 1, pp. 177–182, 1985.
- [24] B. Das, B. D. Tucker, and J. C. Watson, "Acid corrosion analysis of fiberglass," *J. Math. Sci.*, vol. 26, pp. 6606–6612, 1991.
- [25] Q. Qiu and M. Kumosa, "Corrosion of E-glass fibers in acidic environments," *Comp. Sci. Technol.*, vol. 57, pp. 497–507, 1997.
- [26] N. Price and D. Hull, "Propagation of stress corrosion cracks in aligned glass fiber composite materials," *J. Math. Sci.*, vol. 18, p. 2798, 1983.
- [27] M. Kumosa, D. Hull, and J. N. Price, "Acoustic emission from stress corrosion cracks in aligned GRP," *J. Math. Sci.*, vol. 22, pp. 331–336, 1987.
- [28] M. Kumosa, "Acoustic emission monitoring of stress corrosion cracks in aligned GRP," *J. Phys. D: Appl. Phys.*, vol. 20, pp. 69–74, 1987.
- [29] M. Megel, L. Kumosa, T. Ely, D. Armentrout, and M. Kumosa, "Initiation of stress-corrosion cracking in unidirectional glass/polymer composite materials," *Comp. Sci. Tech.*, vol. 61, pp. 231–246, 2001.
- [30] L. Kumosa, D. Armentrout, and M. Kumosa, "An evaluation of the critical conditions for the initiation of stress corrosion cracking in unidirectional e-glass/polymer composites," *Comp. Sci. Technol.*, vol. 61, pp. 615–623, 2001.



**Daniel L. Armentrout** received the bachelor's degree in physics and philosophy from Drake University, Des Moines, IA, in 1985, and the Ph.D. degree in physics from the University of Denver, CO, in 1991.

Currently, Dr. Armentrout is an Associate Research Professor and Lecturer in the Department of Engineering at the University of Denver, CO. His employment experience includes Rocky Flats Environmental Technology Site from 1990 to 1996, where he worked with the SEM on polymer encapsulation of radioactive waste. His special fields

of interest included AE, SEM, and composites.



**Maciej Kumosa** received the Master's and Ph.D. degrees in applied mechanics and materials science from the Technical University of Wroclaw, Poland.

Currently, he is a Professor of Mechanical Engineering at the University of Denver, CO. In the past, Dr. Kumosa worked for several years at the University of Cambridge, U.K. He was also an Associate Professor of Materials Science and Electrical Engineering at the Oregon Graduate Institute, Portland, OR. Dr. Kumosa's research interests include the fracture analysis of advanced composite systems for electrical, aerospace, and space applications. He has performed sponsored research for a variety of private and federal funding agencies in the U.S. including the National Science Foundation, Air Force Office of Scientific Research, NASA, Electric Power Research Institute, and a consortium of U.S. electric utilities. He has also published many publications in numerous composites and applied mechanics international journals.



**Terry S. McQuarrie** received the B.Sc. degree from the University of Oregon, Eugene, and the M.Sc. degree from San Jose State, CA, and the Ph.D. degree from Hamilton University, Evanston, WY, in industrial technology.

Dr. McQuarrie has over 30 years experience in the composite industry. Starting in 1968 at Diamond Shamrock Chemical Co., Redwood City, CA, he was Applications Chemist, Quality Control Supervisor, Research Chemist, and Group Leader of Polyesters.

During this period, he was granted a patent on high-speed resins for the pultrusion process. Later for the Koppers Co., Pittsburgh, PA, he was Industry Manager for Dion Specialty Resins from 1980 to 1987. During this time, he published many articles in various journals. In addition, Dr. McQuarrie has over 15 years of experience in pultrusion industry with Lunastran Co., San Jose, CA, and Glasforms, Inc., San Jose, CA. At Glasforms since 1987, he has developed a full line of epoxy products for use in the nonceramic insulator (NCI) market. This includes diameter from 16 to 88.9 mm for use as suspension and line post products. He has published several articles on the subject of brittle fracture of NCIs.

Dr. McQuarrie is a member of the IEEE Brittle Fracture Task Force and on the steering committee of a consortium of utilities doing basic research on this phenomenon for over eight years currently at the University of Denver.